

D3DR: Lighting-Aware Object Insertion in Gaussian Splatting

Vsevolod Skorokhodov* Nikita Durasov* Pascal Fua
EPFL, Lausanne, Switzerland

{vsevolod.skorokhodov, nikita.durasov, pascal.fua}@epfl.ch

Abstract

Gaussian Splatting has become a popular technique for various 3D Computer Vision tasks, including novel view synthesis, scene reconstruction, and dynamic scene rendering. However, the challenge of natural-looking object insertion, where the object’s appearance seamlessly matches the scene, remains unsolved. In this work, we propose a method, dubbed D3DR, for inserting a 3DGS-parametrized object into 3DGS scenes while correcting its lighting, shadows, and other visual artifacts to ensure consistency, a problem that has not been successfully addressed before. We leverage advances in diffusion models, which, trained on real-world data, implicitly understand correct scene lighting. After inserting the object, we optimize a diffusion-based Delta Denoising Score (DDS)-inspired objective to adjust its 3D Gaussian parameters for proper lighting correction. Utilizing diffusion model personalization techniques to improve optimization quality, our approach ensures seamless object insertion and natural appearance. Finally, we demonstrate the method’s effectiveness by comparing it to existing approaches, achieving 0.5 PSNR and 0.15 SSIM improvements in relighting quality.

1. Introduction

3D object insertion is a computer vision problem that appears when placing a 3D object from one scene into a specific location in another. The task is to adjust the object’s appearance to ensure consistency with the new scene’s lighting, making the insertion appear realistic. Traditional methods rely on physically-based rendering, which requires complex modeling of the scene’s parameters, including texture and lighting. This makes the process slow and demanding while also requiring significant 3D modeling expertise.

Recent advances in Novel View Synthesis (NVS), and in particular the emergence of 3D Gaussian Splatting (3DGS) [11], have transformed scene representation. However, a key challenge when inserting a 3DGS object into

a 3DGS scene — specifically, that the lighting of the inserted object does not match the scene’s lighting, making the insertion appear unrealistic — remains unresolved. Although several approaches have been proposed for other parametrizations [10, 16, 17, 30, 37, 40], they are either not directly applicable to 3DGS or yield unsatisfactory or unrealistic results, highlighting the need for new methods better suited to the 3DGS object insertion task.

In this paper, we show that the 3DGS representation can leverage the power of diffusion models to effectively enforce lighting consistency during object insertion. As shown in Fig. 2, after inserting an object into a new scene we optimize a diffusion-based Delta Denoising Score (DDS)-like objective to refine the object’s appearance, ensuring consistency with the scene surroundings while preserving structural details.

Additionally, we incorporate diffusion model personalization techniques to improve adaptation to specific objects, thereby further enhancing relighting quality. This optimization ensures consistency with the environment while preserving the object’s structure and achieving natural illumination. By using diffusion models trained on large-scale image data, our approach enables effective object relighting without the need for environmental maps or complex material estimation, outperforming existing methods in lighting quality and efficiency for realistic 3D object insertion.

Thus, our two main contributions are as follows:

- We introduce a diffusion-based 3DGS object insertion and relighting method that enforces lighting consistency when integrating 3D objects into 3DGS scenes.
- We collect a diverse dataset of 3DGS scenes and objects and demonstrate through extensive benchmarking that our method significantly outperforms existing approaches in relighting quality.

The code and dataset will be made publicly available.

2. Related works

2.1. 3D Gaussian Splatting

Neural Radiance Fields (NeRFs)[20] have advanced novel view synthesis by modeling scenes as continuous volu-

*Equal contribution.

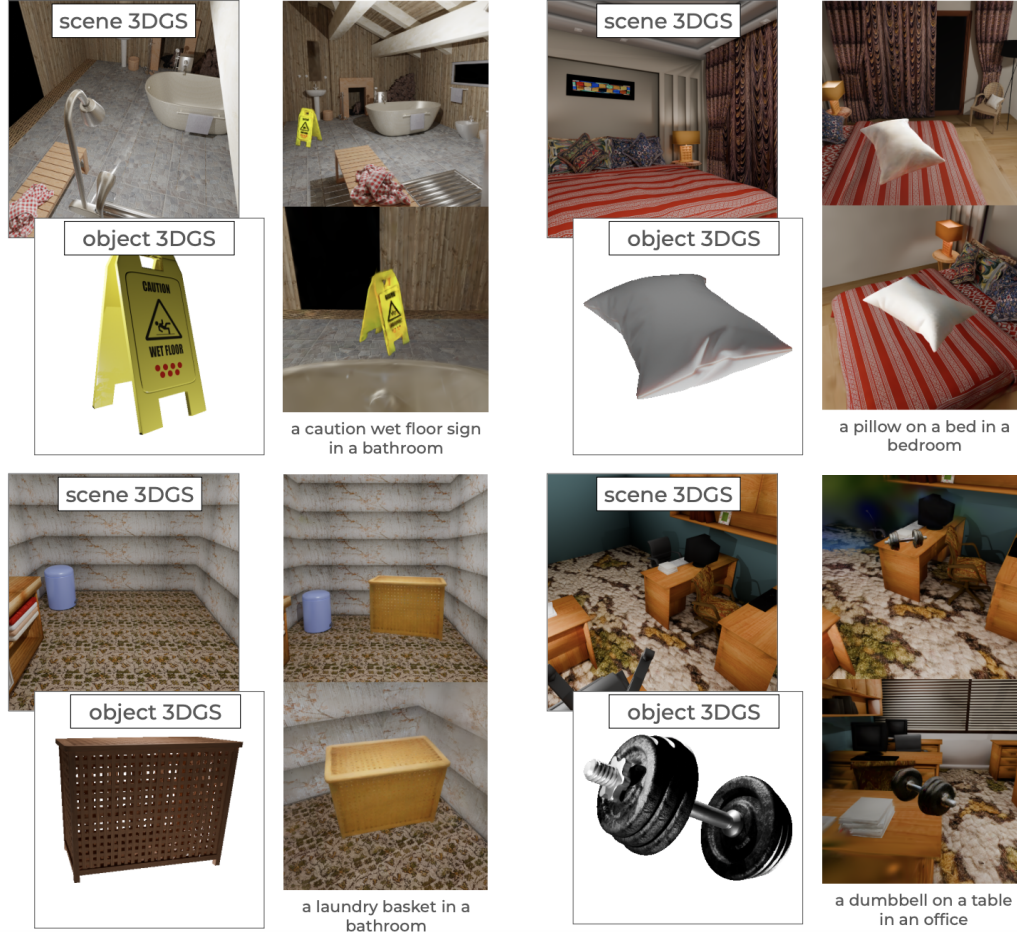


Figure 1. **Overview of the task.** Our method aims to insert an object into a designated location in a scene, both represented in 3DGS parametrization, followed by adjusting the object’s appearance to match the scene’s lighting. The final result is a 3DGS scene that includes both the input scene and the object with corrected lighting.

metric representations using MLP’s. However, NeRFs require expensive optimization and have slow rendering times. Gaussian Splatting (3DGS)[11] offers an efficient alternative by representing scenes explicitly with 3D Gaussians, enabling real-time rendering faster than the quickest NeRFs [21], while preserving visual quality similar to top NeRF methods [1]

In 3DGS, each Gaussian is characterized by its mean μ , covariance Σ , rotation (via quaternion \mathbf{q}), and scaling (via vector \mathbf{s}), opacity o_i , and color information \mathbf{c}_i , which is view-dependent and modeled via spherical harmonics. Rendering is performed by projecting Gaussians onto the image plane and compositing their contributions through alpha blending. In summary, a scene is represented as a collection of Gaussians, each with parameters $\{\mu_i, \mathbf{s}_i, \mathbf{q}_i, o_i, \mathbf{c}_i\}$.

Recent advancements improve its scalability [12], de-blurring [22, 41], dynamic scenes [35], and integration with diffusion-based generative models for 3D content cre-

ation [32] and scene editing [3]. From the best of our knowledge this is the first work addressing 3D Object insertion problem for objects and scenes in 3DGS representation through diffusion-based optimization.

2.2. Diffusion models

Diffusion models [9, 29] have achieved state-of-the-art generative performance in image synthesis [25], inpainting [18], super-resolution [15] and others. Diffusion models denoise an image step-by-step, from a pure gaussian noise to the desired image [9]. Classifier-free guidance [8] is usually applied for text-to-image generation, when the predicted noise is calculated using conditional and unconditional predictions $\varepsilon_\phi^\omega(x; y; t) = \varepsilon_\phi(x; \emptyset; t) + \omega(\varepsilon_\phi(x; y; t) - \varepsilon_\phi(x; \emptyset; t))$, where ε_ϕ is a diffusion model, x is a noisy image, t is a timestep, y is an object representative feature (e.g. text prompt), ω is a guidance scale.

In the context of 3D generation, diffusion models were

successfully applied in DreamFusion [24], where NeRF generation is optimized by computing gradients through a diffusion process. This involves the Score Distillation Sampling (SDS) method, which predicts the noise at each timestep to compute gradients, enabling the optimization of scene parameters such as NeRF’s MLPs. The resulting gradients are then used to update the parameters, as given by:

$$\nabla_{\theta} L_{sds} = \mathbb{E}_{t,\varepsilon} \left[\omega(t) \left(\varepsilon_{\phi}^{\omega}(\alpha_t g(\theta) + \sigma_t \varepsilon; y; t) - \varepsilon \right) \frac{\partial g(\theta)}{\partial \theta} \right], \quad (1)$$

where θ represents scene parameters (such as NeRF’s MLPs or Gaussian parameters in 3DGS), g is a differentiable rendering function, $\omega(t)$, α_t , and σ_t are parameters of the diffusion process, and ε is random Gaussian noise.

Delta Denoising Loss (DDS) [7], an extension of SDS loss originally introduced for image editing tasks, has also been applied to 3D editing [3], addressing the limitation of SDS, which tends to produce blurry and oversaturated results, while DDS reduces these effects [7]. The gradient of the DDS loss with respect to θ is defined in Eq. (2):

$$\nabla_{\theta_{tgt}} L_{dds} = \mathbb{E} \left[\left(\varepsilon_{\phi}^{\omega}(\alpha_t g(\theta_{tgt}) + \sigma_t \varepsilon; y_{tgt}; t) - \varepsilon_{\phi}^{\omega}(\alpha_t g(\theta_{init}) + \sigma_t \varepsilon; y_{init}; t) \right) \frac{\partial g(\theta_{tgt})}{\partial \theta_{tgt}} \right], \quad (2)$$

where θ_{tgt} defines optimizable rendering parameters, θ_{init} defines constant rendering parameters representing the initial state, y_{tgt} is a prompt describing the desired output, and y_{init} is a prompt describing the initial state $g(\theta_{init})$. DDS loss suggests the optimization direction which makes the image aligned with the prompt and reduces the potential bias which appears during SDS optimization [7].

Diffusion Models for Lighting Refinement. Diffusion models transform Gaussian noise into a realistic image, gradually aligning it with the distribution of real images [9]. Trained on large datasets of images with natural lighting, diffusion models implicitly learn its characteristics. Consequently, optimizing with SDS/DDS loss results in more natural illumination in the generated images. An example of this approach can be found in DiffusionLight [23], where the authors in-painted a chrome ball at the center of an image to estimate the environmental light. SDEdit [19] was used to enable in-painting through the diffusion process by adding random Gaussian noise to the image and applying the denoising process. The authors repeated this procedure several times, averaging the results and refining the ball’s appearance. The environmental map derived from the final ball was remarkably precise. We apply a similar strategy for lighting enhancement using DDS loss, as discussed in Sec. 3.3.

2.3. 3DGS Object Insertion

TIP-Editor [43] generates a 3DGS object from scratch in a specific place of 3DGS scene, using a set of scene images and an image of the object, a bounding box, and prompts describing the object and the scene. It firstly personalizes a diffusion model on the scene and on the object using DreamBooth [27] method. Then it generates an object 3DGS from scratch using two SDS losses, one for generating 3DGS and another for making it resemble the object. The method produces realistic glares and shadows on the 3DGS, suggesting that it is a promising direction for 3D object insertion. Because it generates object from scratch, it faces difficulties with generation of big objects Sec. 4.4.

Relightable 3D Gaussians (R3DG) [5] extends classical 3D Gaussian Splatting by learning scene lighting and physically-based parameters such as albedo, roughness, and etc. As a result, inserting a 3DGS object into another 3DGS scene involves learning the lighting and physical parameters for both the object and the scene, then performing a straightforward copy-and-paste operation, and then applying physically-based rendering. However, R3DG encounters challenges distinguishing between actual dark colors and shadows due to a lack of prior knowledge about the object’s intrinsic properties. Furthermore, the method models incident lighting at each Gaussian as the combination of a globally shared environmental light and an indirect light component represented by Gaussian-specific learnable parameters. These parameters depend on the original object scene and thus become invalid when inserting the object into a new scene.

3. Method

3.1. Overall Architecture

In this section, we present our approach for inserting an object into a scene when both are represented by 3D Gaussians (3DGS). In addition to 3DGS-es our approach requires prompts describing an object and a scene for proper diffusion model utilization. An overview of our pipeline is provided in Fig. 2. The method comprises two main steps: first, the *diffusion personalization step* (Sec. 3.2) integrates object-specific information into the diffusion model, enhancing object relighting quality; second, the *DDS step* (Sec. 3.3) leverages the personalized diffusion model from the first step to adjust the object’s appearance, aligning it with the scene lighting. To achieve accurate relighting and avoid color artifacts that typically arise from naive DDS optimization, we introduce a modified version of the DDS loss described in Sec. 3.4.

3.2. Diffusion Personalization

We use DreamBooth [27] for personalized image generation by fine-tuning a pretrained diffusion model with a small set

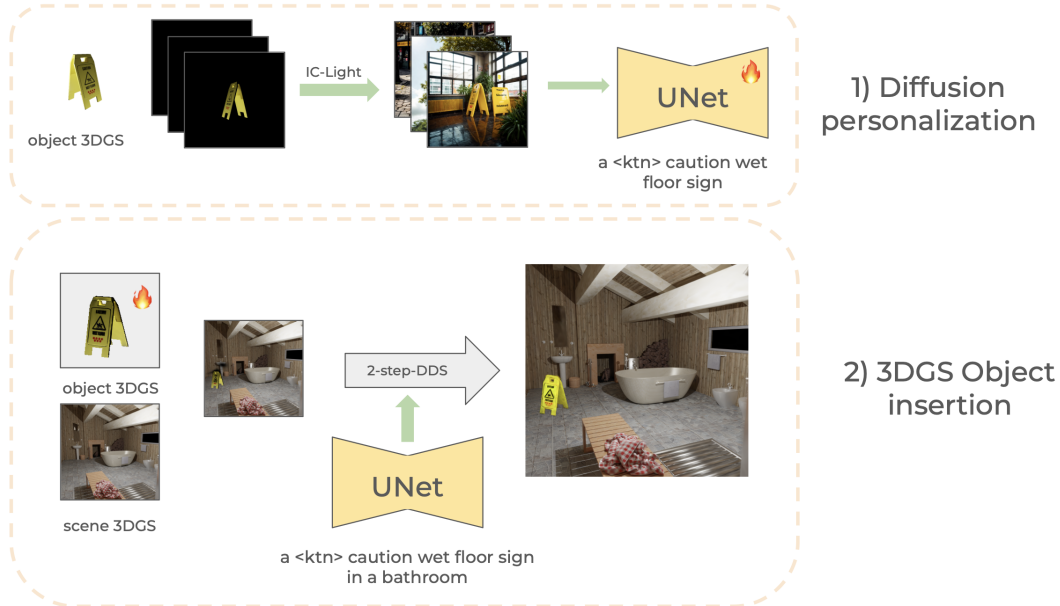


Figure 2. **Pipeline overview.** The method is able to perform 3D Object insertion of a 3DGS object into a 3DGS scene with object light correction. The whole pipeline consists of two steps. 1) a diffusion model is personalized on the object, using framework proposed by DreamBooth [27] and $\langle ktn \rangle$ as a rare token. 2) 2-step-DDS is utilized to adjust the object appearance after 3DGS insertion. Fire means that the parameters are optimized (for UNet during personalization and object parameters during 2-step-DDS).

of object images. To prevent overfitting and maintain generalization, DreamBooth employs *class preservation*, generating additional class-specific images for training. However, a classical DreamBooth personalization tends to overfit to a single lighting condition, as discussed in Sec. 4.5. To mitigate this, we utilize IC-Light [39], which synthesizes object images under varied illumination and backgrounds. IC-Light takes an object image, an object prompt, a background prompt, and lighting direction as inputs. Our approach involves sampling N random viewpoints to render object images via 3D Gaussian Splatting (3DGS), selecting N random backgrounds from 20 predefined environments (e.g., *kitchen, beach, forest, library*), and choosing lighting directions from two options (*right, left*). IC-Light then creates diverse images combining these elements. Finally, we fine-tune the diffusion model using DreamBooth with this varied image set. More details on personalization parameters are provided in Sec. 4.

3.3. Delta Denoising Score (DDS)

As we discussed in Sec. 3.2, DiffusionLight [23] demonstrated that a chrome ball has correct lighting after inpainting in an image through the image-editing pipeline Sec. 2.2. Thus, it is reasonable to hypothesize that DDS-based object inpainting would similarly correct the object’s lighting. Our experiments, described in Sec. 4, confirm that inpainting indeed improves object lighting.

However, image editing using classical DDS strongly de-

pends on the object’s initial lighting conditions. As shown in our experiments Sec. 4, classical DDS does not enhance the object’s appearance during insertion in the 2D scenario. To address this limitation, we propose a modified initialization strategy for DDS that improves object appearance upon insertion.

For notations please refer to Sec. 2.2. Consider an image of a scene without an object as img_{scene} and an image of the same scene containing an object with incorrect appearance as $img_{scene+obj}$. When we set images $g(\theta_{init}) = g(\theta_{tgt}) = img_{scene}$, prompts $y_{tgt} = an \langle object-description \rangle in a \langle scene-description \rangle$ and $y_{init} = a \langle scene-description \rangle$, the DDS optimization becomes an image inpainting task, generating the object within the scene [7]. By setting $g(\theta_{init}) = img_{scene}$ and $g(\theta_{tgt}) = img_{scene+obj}$, we also obtain an inpainting scenario, but the initialization of the optimizable image $g(\theta_{tgt})$ already includes our target object, which is great because DDS editing needs only to change object lighting, since the target object is already presented on the image.

To sum up, our proposed initialization approach differs from classical initialization only in a way that $g(\theta_{init}) = img_{scene}$ but not $g(\theta_{obj+scene})$. Therefore, our DDS optimization for slightly differs from classical DDS and includes the following steps:

1. Sample a random viewpoint and render two views: $g(\theta_{tgt})$ and $g(\theta_{init})$.
2. Sample Gaussian noise $\varepsilon \sim \mathcal{N}(0, I)$ and timestep $t \sim$

$U(1, T)$.

3. Compute gradient $\nabla_{\theta_{tgt}} L_{dds}$ Eq. (2) at a single (ε, t) pair.
4. Backpropagate and update θ_{tgt} .
5. Repeat from step 1.

3.4. DDS Optimization

In SDS Sec. 2.2, we previously referred to $g(\theta)$ as an image. Modern diffusion models operate in latent space, improving efficiency without sacrificing quality. Thus, $g(\theta)$ is actually a latent vector obtained by encoding an image using a Variational Autoencoder (VAE) [13]. SDS optimization usually occurs in latent space: the latent representation is optimized with the SDS loss and then decoded back to image space. Direct SDS optimization in image space typically introduces noise and artifacts due to inherent ambiguities [32]. Interestingly, this problem does not frequently occur when SDS generates 3D representations like NeRFs or 3D Gaussian Splatting (3DGS) [24, 32], though some recent 3DGS editing methods still face this issue [3, 36]. We also meet this problem during naive DDS optimization, and we present an approach to eliminate this issue.

We propose a pipeline for inserting a 3DGS object into a 3DGS scene while aligning its appearance with scene lighting. Since the object is already represented in 3DGS, directly transferring its gaussians’ parameters ensures correct geometry insertion, requiring adjustments only for Gaussian colors and spherical harmonics (SH). However, directly applying this DDS optimization of color coefficients introduces SDS-related noise. To resolve this, we propose a two-stage optimization strategy inspired by the fact that latent-space SDS optimization does not produce noisy images [24]. For 2D generation using SDS, we perform the following: first, initialize the 2D image as random noise, encode this noisy image into latent space, and optimize only the latent representation for several iterations without altering the image parameters (step 1). After decoding the latent (which does not contain noise artifacts) back into image space, we apply several steps of MSE/MAE optimization to adjust the original image closer to the decoded latent (step 2). Finally, we repeat these two steps. This method significantly reduces artifacts and improves efficiency. Our detailed optimization procedure is provided as pseudocode in Algorithm 1. Extensive experimental results demonstrating our method’s effectiveness for 3DGS are shown in Sec. 4.5, with additional 2D image examples available in the supplementary material.

4. Experimental results

4.1. Datasets

Our dataset is built upon SceneNet [6], with additional objects sourced from BlenderKit [2] and textures from

Algorithm 1 2-step-DDS optimization

```

1: procedure 2-STEP-DDS(unet, vae,  $y_{tgt}$ ,  $y_{init}$ ,
    $\theta_{tgt}$ ,  $\theta_{init}$ ,
   steps_latent, steps_image, num_iters, lr)
2:    $\theta = \theta_{tgt}$ 
3:   optimizer = Adam( $\theta$ .state_dict())
4:   for  $i$  in  $[1 \dots \lceil \frac{num\_iters}{steps\_image} \rceil]$  do
5:     latent = vae.encode( $g(\theta)$ ).detach()
6:      $x_{init} = \text{vae.encode}(g(\theta_{init})).\text{detach}()$ 
7:     # step 1 — SGD latent optimization
8:     for  $j$  in  $[1 \dots steps\_latent]$  do
9:        $t \sim \mathcal{U}(1, T)$ ,  $\varepsilon \sim \mathcal{N}(0, I)$ 
10:       $z_{tgt} = \alpha_t \text{latent} + \sigma_t \varepsilon$ 
11:       $z_{init} = \alpha_t x_{init} + \sigma_t \varepsilon$ 
12:      calculate  $\nabla_{\theta} L_{dds}$  Eq. (2) using unet,
    $t, z_{tgt}, y_{tgt}, z_{init}, y_{init}$ 
13:      latent = latent - lr · gradDDS
14:    end for
15:    # step 2 — Adam  $\theta$  optimization
16:    image_opt = vae.decode(latent)
17:    for  $j$  in  $[1 \dots steps\_image]$  do
18:      optimizer.zero_grad()
19:      loss = L1( $g_{tgt}(\theta, p)$ , image_opt)
20:      loss.backward()
21:      optimizer.step() #  $\theta$  is updated
22:    end for
23:  end for
24:  return  $\theta$ 
25: end procedure

```

Freepik [4]. It is strictly for research purposes. The dataset includes 10 indoor scenes: *bathroom_1*, *bathroom_2*, *bedroom_1*, *bedroom_2*, *kitchen_1*, *kitchen_2*, *living_room_1*, *living_room_2*, *office_1*, *office_2*. Each scene contains at least one placed object, such as a *caution wet floor sign* in *bathroom_1*, a *laundry basket* in *bathroom_2*, etc. We consider three rendering settings: *object*, *scene*, and *object + scene*, resulting in 30 sets of images — only objects (10 sets), objects in scenes (10 sets), only scenes (10 sets). For further details on the dataset, including specific rendering settings and point cloud generation methods, please refer to the supplementary material.

4.2. 2D Object insertion using DDS

DDS relies on the initial object’s lighting conditions during editing, causing the edited object to inherit these conditions. To illustrate this, we use the standard DDS pipeline to transform a cup into a statue head (see Fig. 3). When the cup has correct lighting, the resulting statue head appears realistic; however, incorrect initial lighting leads to similar issues in the edited object.

To mitigate this issue, we propose a different initializa-



Figure 3. **DDS image editing and lighting dependence.** The first column shows the initial images of a cup: the top image has correct lighting, while the bottom one has incorrect lighting. The second column presents the edited outputs using the classical DDS loss. The initial prompt y_{init} is *a cup on a plate*, and the target prompt y_{tgt} is *a statue head on a plate*. The results demonstrate that DDS inherits object lighting: the statue head in the top row has correct lighting, while the one in the bottom row retains the incorrect lighting of the cup.

tion for θ_{init} described in Sec. 3.3 to prevent undesired lighting inheritance and improves object insertion in 2D images. Utilizing this initialization, DDS optimization can refine the object’s appearance after insertion into a new scene. The Fig. 4 illustrates the optimization process of a cup inserted into an image. Initially, the cup appears misaligned with the scene lighting, but as optimization progresses, it becomes visually consistent with the surrounding environment.

To further enhance geometric consistency, we integrate a depth-conditioned ControlNet [38]. Here, y is not merely a text prompt but a structured input: {prompt, ControlNet condition}. Additionally, we apply a mask to constrain gradient updates to the cup, ensuring that background pixels remain unchanged.

4.3. Implementation details

Our experiments are conducted on a single NVIDIA V100 32GB GPU. We use DN-Splatter [33] to train the 3DGS representation of objects and scenes, as it outperforms the classical 3DGS [11] pipeline in novel view synthesis (NVS). For object 3DGS, we do not use normal and depth reg-

ularization losses, as they degrade the final 3DGS quality. Similarly, for scene 3DGS, we omit the depth regularization loss. We train the 3DGS representations for 30,000 iterations using the default DN-splatter parameters. Our implementation is based on nerfstudio [31] framework. The object-describing prompt $\langle object_desc \rangle$ and scene-describing $\langle scene_desc \rangle$ prompt are user defined.

We use Stable Diffusion 2.1 [26] from Hugging Face [34]. We generate $N = 32$ images using IC-Light [39], following the procedure described in Sec. 3.2. For class preservation Sec. 3.2, we generate 200 images of the same object class. During DreamBooth [27] personalization, we randomly select an IC-Light-generated image with a probability of 0.7 and a class-preservation image with a probability of 0.3. The fine-tuning prompts are a $\langle object_desc \rangle$ for class-preservation images and a $\langle ktn \rangle \langle object_desc \rangle$ for IC-Light images. A token $\langle ktn \rangle$ is used in DreamBooth for personalization. We fine-tune the Stable Diffusion model for 500 iterations using a batch size of 4, AdamW optimizer with $weight_decay 1 \cdot 10^{-2}$, a learning rate of $5 \cdot 10^{-6}$, and a constant learning rate scheduler. The fine-tuned model is then used for 2-step-DDS optimization. This step took approximately 30 minutes.

For 2-step-DDS part, we initialize the object’s colors as the mean of all object colors and set its spherical harmonics (SH) coefficients to zero. We set $y_{tgt,prompt} = a \langle object_desc \rangle$ in a $\langle scene_desc \rangle$, $y_{init,prompt} = a \langle scene_desc \rangle$. The algorithm performs 20,000 training steps with $sh_degree_interval = 5000$, progressively activating a new SH degree. We set $steps_image = 256$, $steps_latent = 16$, and $guidance_scale = 7.5$. We use the Depth ControlNet implementation from Hugging Face and set $controlnet_conditioning_scale$ to 1.0. During the *step 1* of 2-step-DDS (latent optimization), we set $latent_lr = 0.1$. Object colors are optimized using Adam with a learning rate of 0.0025 and exponential learning rate decay, while object spherical harmonics are optimized with Adam at a learning rate of 0.000125. For the image loss, we use only L1 loss, omitting SSIM, as standard in 3DGS training. The 2-step-DDS optimization takes about 20 minutes per scene.

4.4. Comparing with other methods

We compare our approach against TIP-Editor [43] and Relightable 3D Gaussian (R3DG) [5]. We observe that TIP-Editor fails to generate objects when the scene 3DGS is trained with DN-Splatter, requiring us to use its original training pipeline instead. We follow their default training parameters and ensure that the prompts describing the scenes remain identical between TIP-Editor and our method. The average total training time for TIP-Editor, excluding 3DGS scene training, consists of 20 minutes for scene personalization, 3 minutes for object personalization, 115 minutes for SDS generation, and 2 minutes for SDS



Figure 4. **DDS refines object appearance after insertion.** The first row illustrates the optimization process for a cup inserted into an image. The rightmost image represents the ground-truth cup on a plate. The second image shows an inserted cup with incorrect lighting, despite identical global lighting conditions. Images 3–7 depict the cup’s gradual adaptation through DDS optimization. The second row presents a similar experiment under different lighting conditions. The final results closely match the appearance of the ground-truth cups.

		bathroom_1	bathroom_2	bedroom_1	bedroom_2	kitchen_1	kitchen_2	living_room_1	living_room_2	office_1	office_2	average
PSNR _{part} (↑)	D3DR	6.161	11.311	8.415	7.892	14.422	6.927	4.737	13.031	7.242	8.489	8.863
	R3DG	8.583	10.595	8.023	6.164	8.860	3.467	12.763	8.491	9.236	7.877	8.406
	TIP-Editor	11.344	8.587	5.875	4.128	8.846	6.799	15.424	7.154	10.987	2.907	8.205
SSIM _{part} (↑)	D3DR	0.554	0.393	0.816	0.447	0.487	0.400	0.565	0.571	0.696	0.470	0.540
	R3DG	0.394	0.511	0.694	0.447	0.193	0.279	0.620	0.282	0.421	0.354	0.419
	TIP-Editor	0.447	0.298	0.455	0.233	0.341	0.283	0.666	0.320	0.642	0.322	0.401
CTIS (↑)	ours	0.622	0.623	0.646	0.634	0.624	0.627	0.634	0.614	0.629	0.616	0.627
	R3DG	0.611	0.621	0.645	0.630	0.629	0.626	0.612	0.616	0.627	0.614	0.623
	TIP-Editor	0.603	0.608	0.625	0.631	0.626	0.626	0.602	0.608	0.628	0.612	0.617
DTIS (↑)	D3DR	0.527	0.503	0.509	0.503	0.500	0.502	0.537	0.506	0.500	0.506	0.509
	R3DG	0.518	0.505	0.508	0.500	0.506	0.501	0.511	0.508	0.500	0.505	0.506
	TIP-Editor	0.505	0.494	0.499	0.499	0.503	0.500	0.502	0.500	0.500	0.500	0.500

Table 1. **Comparison with other methods.** The first column represents metrics names, the second column represents methods names, columns 3-12 represent scenes, the last column contains averages across rows. The first three rows represent PSNR_{part}, the second three rows represent SSIM_{part}, the third three rows represent CTIS, and the last three rows represent DTIS. **Bold** numbers represent the best across methods. ↑ represents that the metric is better if the value is greater. D3DR outperforms other methods by a significant margin.

refinement, summing to 140 minutes. R3DG requires surface normals, which are unavailable in our object 3DGS. To ensure fair comparison, we adopt their training pipeline for both object and scene 3DGS. For scene training, we use the script provided for the Tanks and Temples dataset [14], as this dataset is closest to ours. However, we observe that their 3DGS method begins producing floating points after 10,000 iterations, so we take a checkpoint at this stage. We then proceed with their second training step for 20,000 iterations using their official script. For object training, we use the script provided for the NeRF Synthetic Dataset. The total average training time for R3DG, excluding 3DGS scene and object generation, consists of 150 minutes for scene physical parameter learning and 35 minutes for object physical parameter learning, summing to 185 minutes.

The quantitative comparison is presented in Tab. 1. We report PSNR_{part}, which measures PSNR on object pixels only, and SSIM_{part}, which measures SSIM within the object bounding box. Additionally, following prior works [28, 42], we compute CLIP-based metrics. CTIS represents the cosine similarity between CLIP features of the prompt and the generated image, while DTIS measures the cosine similarity between the CLIP features of the target and initial images, reflecting the alignment of transformations. Both CTIS and DTIS are normalized to the range [0, 1]. Some generated examples are shown in Fig. 5, please refer to supplementary for more generation results. Our method consistently outperforms TIP-Editor and R3DG across all evaluated metrics on average. Furthermore, the Tab. 2 shows that on average our method not only trains almost three

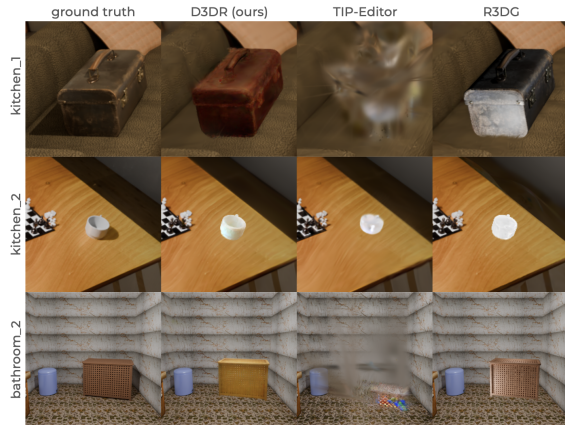


Figure 5. **Comparison with other methods.** The first column shows ground truth object insertions, the second column presents results from our method, the third column shows TIP-Editor results, and the fourth column displays R3DG results. The rows represent different scenes, such as *kitchen_1*, *kitchen_2*, and *bathroom_2*.

times faster, but also requires less memory and less gaussians to represent scenes. TIP-Editor struggles with gener-

	Time, minutes (↓)	Memory, GB (↓)	N, 10^6 (↓)
D3DR	50	0.076	0.33
TIP-Editor	140	0.097	1.87
R3DG	185	0.955	1.97

Table 2. **Time and memory comparisons.** The first column represents methods, the second column is average training time, the third column is average memory requirements to store gaussians, the fourth memory is the number of gaussians.

ating large objects because it reconstructs the object 3DGS from scratch using SDS, whereas our method directly leverages existing 3DGS objects representations. R3DG, on the other hand, suffers from issues related to incident light and albedo, as discussed in Sec. 2.3, leading to suboptimal object insertion quality.

4.5. Ablation studies

Impact of IC-Light on Personalization. Personalization requires observing the object under diverse lighting conditions. Without IC-Light, the diffusion model overfits to a single lighting setup, resulting in unrealistic appearances that do not match the scene. As shown in Fig. 6, omitting IC-Light leads to inaccurate shadows and incorrect lighting, highlighted by red circles.

Impact of 2-step-DDS. Figure Fig. 6 illustrates the impact of standard DDS optimization on *bathroom_1* and

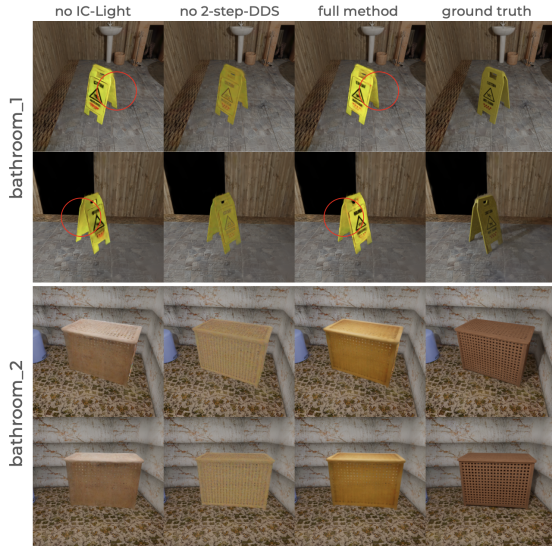


Figure 6. **Ablation studies on IC-Light and 2-step-DDS.** Each row represents a different camera ppose. The first two rows correspond to the *bathroom_1* scene, while the last two correspond to the *bathroom_2* scene. The first column shows results without IC-Light, the second without 2-step-DDS, the third with our full method, and the fourth is the ground truth. Red circles highlight key differences.

bathroom_2. Without 2-step-DDS (second column), noticeable noise patterns emerge. Additionally, our approach eliminates the need for gradient computation through the VAE, significantly improving efficiency — our method completes 20,000 training steps in about 20 minutes, whereas standard DDS requires 80 minutes for the same number of steps.

For ablations studies on diffusion personalization and color average initialization please refer to the supplementary material.

5. Conclusion

We have introduced D3DR, a diffusion-driven method designed to address the previously unsolved problem of natural-looking object insertion within 3D Gaussian Splatting scenes. By formulating the insertion task as an optimization of Gaussian parameters guided by a diffusion-based Delta Denoising Score (DDS)-inspired objective, our approach effectively corrects lighting, shadows, and visual artifacts to produce consistent and visually coherent results. Leveraging diffusion model personalization further enhances optimization stability and convergence, achieving superior visual realism compared to existing methods. Empirical evaluations demonstrate notable improvements in relighting quality, quantitatively surpassing baseline approaches by 0.5 PSNR and 0.15 SSIM. We believe our method paves the way toward more realistic and versatile 3D object insertion and manipulation in neural graphics ap-

plications.

References

- [1] Jonathan T Barron, Ben Mildenhall, Matthew Tancik, Peter Hedman, Ricardo Martin-Brualla, and Pratul P Srinivasan. Mip-nerf: A multiscale representation for anti-aliasing neural radiance fields. In *Proceedings of the IEEE/CVF international conference on computer vision*, pages 5855–5864, 2021. 2
- [2] BlenderKit Online Community. *BlenderKit*, 2024. 5
- [3] Yiwen Chen, Zilong Chen, Chi Zhang, Feng Wang, Xiaofeng Yang, Yikai Wang, Zhongang Cai, Lei Yang, Huaping Liu, and Guosheng Lin. Gaussianeditor: Swift and controllable 3d editing with gaussian splatting. In *Proceedings of the IEEE/CVF conference on computer vision and pattern recognition*, pages 21476–21485, 2024. 2, 3, 5
- [4] Freepik. *Freepik*, 2024. 5
- [5] Jian Gao, Chun Gu, Youtian Lin, Zhihao Li, Hao Zhu, Xun Cao, Li Zhang, and Yao Yao. Relightable 3d gaussians: Realistic point cloud relighting with brdf decomposition and ray tracing. In *European Conference on Computer Vision*, pages 73–89. Springer, 2025. 3, 6
- [6] Ankur Handa, Viorica Pătrăucean, Vijay Badrinarayanan, Simon Stent, and Roberto Cipolla. Scenenet: Understanding real world indoor scenes with synthetic data. In *arXiv*, 2015. 5
- [7] Amir Hertz, Kfir Aberman, and Daniel Cohen-Or. Delta denoising score. In *Proceedings of the IEEE/CVF International Conference on Computer Vision*, pages 2328–2337, 2023. 3, 4
- [8] Jonathan Ho and Tim Salimans. Classifier-free diffusion guidance. *arXiv preprint arXiv:2207.12598*, 2022. 2
- [9] Jonathan Ho, Ajay Jain, and Pieter Abbeel. Denoising diffusion probabilistic models. *Advances in neural information processing systems*, 33:6840–6851, 2020. 2, 3
- [10] Haian Jin, Isabella Liu, Peijia Xu, Xiaoshuai Zhang, Songfang Han, Sai Bi, Xiaowei Zhou, Zexiang Xu, and Hao Su. Tensoir: Tensorial inverse rendering. In *Proceedings of the IEEE/CVF Conference on Computer Vision and Pattern Recognition*, pages 165–174, 2023. 1
- [11] Bernhard Kerbl, Georgios Kopanas, Thomas Leimkühler, and George Drettakis. 3d gaussian splatting for real-time radiance field rendering. *ACM Trans. Graph.*, 42(4):139–1, 2023. 1, 2, 6
- [12] Bernhard Kerbl, Andreas Meuleman, Georgios Kopanas, Michael Wimmer, Alexandre Lanvin, and George Drettakis. A hierarchical 3d gaussian representation for real-time rendering of very large datasets. *ACM Transactions on Graphics*, 43(4), 2024. 2
- [13] Diederik P Kingma, Max Welling, et al. Auto-encoding variational bayes, 2013. 5
- [14] Arno Knapitsch, Jaesik Park, Qian-Yi Zhou, and Vladlen Koltun. Tanks and temples: Benchmarking large-scale scene reconstruction. *ACM Transactions on Graphics*, 36(4), 2017. 7
- [15] Haoying Li, Yifan Yang, Meng Chang, Shiqi Chen, Huajun Feng, Zhihai Xu, Qi Li, and Yueting Chen. Srdiff: Single image super-resolution with diffusion probabilistic models. *Neurocomputing*, 479:47–59, 2022. 2
- [16] Zhengqin Li, Mohammad Shafiei, Ravi Ramamoorthi, Kalyan Sunkavalli, and Manmohan Chandraker. Inverse rendering for complex indoor scenes: Shape, spatially-varying lighting and svbrdf from a single image. In *Proceedings of the IEEE/CVF conference on computer vision and pattern recognition*, pages 2475–2484, 2020. 1
- [17] Ruofan Liang, Zan Gojcic, Merlin Nimier-David, David Acuna, Nandita Vijaykumar, Sanja Fidler, and Zian Wang. Photorealistic object insertion with diffusion-guided inverse rendering. In *European Conference on Computer Vision*, pages 446–465. Springer, 2024. 1
- [18] Andreas Lugmayr, Martin Danelljan, Andres Romero, Fisher Yu, Radu Timofte, and Luc Van Gool. Repaint: Inpainting using denoising diffusion probabilistic models. In *Proceedings of the IEEE/CVF conference on computer vision and pattern recognition*, pages 11461–11471, 2022. 2
- [19] Chenlin Meng, Yutong He, Yang Song, Jiaming Song, Jiajun Wu, Jun-Yan Zhu, and Stefano Ermon. Sdedit: Guided image synthesis and editing with stochastic differential equations. *arXiv preprint arXiv:2108.01073*, 2021. 3
- [20] Ben Mildenhall, Pratul P Srinivasan, Matthew Tancik, Jonathan T Barron, Ravi Ramamoorthi, and Ren Ng. Nerf: Representing scenes as neural radiance fields for view synthesis. *Communications of the ACM*, 65(1):99–106, 2021. 1
- [21] Thomas Müller, Alex Evans, Christoph Schied, and Alexander Keller. Instant neural graphics primitives with a multiresolution hash encoding. *ACM transactions on graphics (TOG)*, 41(4):1–15, 2022. 2
- [22] Cheng Peng, Yutao Tang, Yifan Zhou, Nengyu Wang, Xijun Liu, Deming Li, and Rama Chellappa. Bags: Blur agnostic gaussian splatting through multi-scale kernel modeling. In *European Conference on Computer Vision*, pages 293–310. Springer, 2024. 2
- [23] Pakkapon Phongthawee, Worameth Chinchuthakun, Nontaphat Sinsunthithet, Varun Jampani, Amit Raj, Pramook Khungurn, and Supasorn Suwajanakorn. Diffusionlight: Light probes for free by painting a chrome ball. In *Proceedings of the IEEE/CVF conference on computer vision and pattern recognition*, pages 98–108, 2024. 3, 4
- [24] Ben Poole, Ajay Jain, Jonathan T Barron, and Ben Mildenhall. Dreamfusion: Text-to-3d using 2d diffusion. *arXiv preprint arXiv:2209.14988*, 2022. 3, 5
- [25] Aditya Ramesh, Prafulla Dhariwal, Alex Nichol, Casey Chu, and Mark Chen. Hierarchical text-conditional image generation with clip latents. *arXiv preprint arXiv:2204.06125*, 1(2):3, 2022. 2
- [26] Robin Rombach, Andreas Blattmann, Dominik Lorenz, Patrick Esser, and Björn Ommer. High-resolution image synthesis with latent diffusion models. In *Proceedings of the IEEE/CVF conference on computer vision and pattern recognition*, pages 10684–10695, 2022. 6
- [27] Nataniel Ruiz, Yuanzhen Li, Varun Jampani, Yael Pritch, Michael Rubinstein, and Kfir Aberman. Dreambooth: Fine tuning text-to-image diffusion models for subject-driven

- generation. In *Proceedings of the IEEE/CVF conference on computer vision and pattern recognition*, pages 22500–22510, 2023. 3, 4, 6
- [28] Mohamad Shahbazi, Liesbeth Claessens, Michael Niemeyer, Edo Collins, Alessio Tonioni, Luc Van Gool, and Federico Tombari. Inerf: text-driven generative object insertion in neural 3d scenes. *arXiv preprint arXiv:2401.05335*, 2024. 7
- [29] Yang Song, Jascha Sohl-Dickstein, Diederik P Kingma, Abhishek Kumar, Stefano Ermon, and Ben Poole. Score-based generative modeling through stochastic differential equations. *arXiv preprint arXiv:2011.13456*, 2020. 2
- [30] Yizhi Song, Zhifei Zhang, Zhe Lin, Scott Cohen, Brian Price, Jianming Zhang, Soo Ye Kim, and Daniel Aliaga. Objectstitch: Generative object compositing. *arXiv preprint arXiv:2212.00932*, 2022. 1
- [31] Matthew Tancik, Ethan Weber, Evonne Ng, Ruilong Li, Brent Yi, Terrance Wang, Alexander Kristoffersen, Jake Austin, Kamyar Salahi, Abhik Ahuja, et al. Nerfstudio: A modular framework for neural radiance field development. In *ACM SIGGRAPH 2023 Conference Proceedings*, pages 1–12, 2023. 6
- [32] Jiaxiang Tang, Jiawei Ren, Hang Zhou, Ziwei Liu, and Gang Zeng. Dreamgaussian: Generative gaussian splatting for efficient 3d content creation. *arXiv preprint arXiv:2309.16653*, 2023. 2, 5
- [33] Matias Turkulainen, Xuqian Ren, Iaroslav Melekhov, Otto Seiskari, Esa Rahtu, and Juho Kannala. Dn-splatter: Depth and normal priors for gaussian splatting and meshing. *arXiv preprint arXiv:2403.17822*, 2024. 6
- [34] T Wolf. Huggingface’s transformers: State-of-the-art natural language processing. *arXiv preprint arXiv:1910.03771*, 2019. 6
- [35] Guanjun Wu, Taoran Yi, Jiemin Fang, Lingxi Xie, Xiaopeng Zhang, Wei Wei, Wenyu Liu, Qi Tian, and Xinggang Wang. 4d gaussian splatting for real-time dynamic scene rendering. In *Proceedings of the IEEE/CVF conference on computer vision and pattern recognition*, pages 20310–20320, 2024. 2
- [36] Hanyuan Xiao, Yingshu Chen, Huajian Huang, Haolin Xiong, Jing Yang, Pratusha Prasad, and Yajie Zhao. Localized gaussian splatting editing with contextual awareness. *arXiv preprint arXiv:2408.00083*, 2024. 5
- [37] Keyang Ye, Hongzhi Wu, Xin Tong, and Kun Zhou. A real-time method for inserting virtual objects into neural radiance fields. *IEEE Transactions on Visualization and Computer Graphics*, 2024. 1
- [38] Lvmin Zhang, Anyi Rao, and Maneesh Agrawala. Adding conditional control to text-to-image diffusion models. In *Proceedings of the IEEE/CVF International Conference on Computer Vision*, pages 3836–3847, 2023. 6
- [39] Lvmin Zhang, Anyi Rao, and Maneesh Agrawala. Scaling in-the-wild training for diffusion-based illumination harmonization and editing by imposing consistent light transport. In *The Thirteenth International Conference on Learning Representations*, 2025. 4, 6
- [40] Xiuming Zhang, Pratul P Srinivasan, Boyang Deng, Paul Debevec, William T Freeman, and Jonathan T Barron. Nerfactor: Neural factorization of shape and reflectance under an unknown illumination. *ACM Transactions on Graphics (TOG)*, 40(6):1–18, 2021. 1
- [41] Lingzhe Zhao, Peng Wang, and Peidong Liu. Bad-gaussians: Bundle adjusted deblur gaussian splatting. In *European Conference on Computer Vision*, pages 233–250. Springer, 2024. 2
- [42] Hongliang Zhong, Can Wang, Jingbo Zhang, and Jing Liao. Generative object insertion in gaussian splatting with a multi-view diffusion model. *arXiv preprint arXiv:2409.16938*, 2024. 7
- [43] Jingyu Zhuang, Di Kang, Yan-Pei Cao, Guanbin Li, Liang Lin, and Ying Shan. Tip-editor: An accurate 3d editor following both text-prompts and image-prompts. *ACM Transactions on Graphics (TOG)*, 43(4):1–12, 2024. 3, 6

Appendices

A. Rendering Details and Point Cloud Generation

In this section, we provide detailed descriptions of the rendering settings and the point cloud generation methods used for the dataset.

A.1. Rendering Settings

We consider three rendering settings:

- **Object Rendering:** The object is placed at the origin with zero Euler angles, and the scene and its lighting are hidden. A set of point lights is placed around the object, with the number of lights increasing for larger objects. The camera follows a circular trajectory with random variations in distance and look-at position to introduce natural perturbations. Both images and object masks are generated.
- **Object + Scene Rendering:** The camera moves around a selected look-at point within the scene, with small random shifts similar to the *object* setting. Both the object and the scene are rendered.
- **Scene Rendering:** The object is hidden, and the camera follows the same trajectory as in the *object + scene* setting, but only the scene is rendered.

A.2. Point Cloud Generation

Gaussian Splatting requires a sparse set of initialization points. Existing methods, such as those in [?], typically place points only at the mesh corners, which can result in an uneven distribution. To address this, we propose an improved point cloud generation method in Blender, which integrates three sampling strategies:

1. **Surface Area Sampling:** A scene object is sampled based on its surface area, using $Volume^{2/3}$ instead of ordinary area to avoid over-representing thin structures like plant leaves. Then, a triangle is selected from the object’s mesh proportional to its area, and a point is sampled uniformly on the triangle.
2. **Uniform Triangle Sampling:** A scene object is sampled, followed by the selection of a triangle from its mesh. Finally, a point is sampled uniformly on the triangle.
3. **Bounding Box Sampling:** A point is sampled within the scene’s bounding box, the closest mesh triangle is found, and a point is sampled uniformly on that triangle.

A.3. Rendering and Point Cloud Generation Details

We use the *cycles* renderer with 256 samples per image, generating 250 images per setting. Object masks are rendered for *object* and *object + scene* settings.

For sparse point clouds, we sample:

- 10,000 points for *object*
- 5,000 points for *object + scene*
- 50,000 points for *scene*

Dataset images are shown in Fig. 7.

B. Tiny Cup Dataset

We use a small dataset of four real images Fig. 8 and two artificially generated images to analyze how DDS relies on object appearance for editing. The real images depict a cup in a room under two different lighting conditions, with an additional pair of images showing the same room under the same lighting conditions but without the cup. The artificial images are created by inserting the cup, captured under one lighting condition, into an image of the room with a different illumination.

C. 2-step-SDS image generation

We conduct image generation in image space using our proposed 2-step-SDS approach, with results shown in Fig. 10. Classical SDS optimization in image space introduces noticeable noise artifacts, whereas both SDS optimization in latent space and our 2-step-SDS method effectively mitigate this issue. We set the classifier-free guidance coefficient to $\omega = 15$ and perform 1,000 optimization steps for each method. SDS latent optimization and 2-step-SDS complete image generation in approximately 1 minute, while classical SDS in image space requires 2 minutes.

D. More ablation studies

Impact of Personalization. Personalization plays a crucial role in preserving object textures. We conduct ablation studies by replacing the personalized model with a standard Stable Diffusion model. When using average color initialization, the final object textures deviate significantly from the original object textures. However, even without average initialization, texture consistency is not fully preserved. For example, in *bathroom_1*, the caution wet floor sign retains correct textures on one side, while the other side exhibits completely different textures. Additionally, black Gaussian artifacts appear along the border and persist throughout optimization.

Impact of Mean Initialization. Initializing an object’s colors as the average of all its colors reduces lighting bias at the start of optimization. Without this initialization, the final object appearance becomes less realistic, as shown in Fig. 11. This effect is particularly evident in *bathroom_2*, where the overall realism decreases. In *bathroom_1*, the absence of mean initialization results in less visible shadows. Interestingly, when neither personalization nor mean initialization is used, the object appearance remains visually plausible, but the textures become inconsistent.



Figure 7. **Our dataset.** The dataset consists of 30 sets of images and point clouds, categorized into three groups: 10 sets for objects, 10 sets for objects within scenes, and 10 sets for scenes alone. An item is a random image from the appropriate set. Each row corresponds to different images captured at the same location, while each column groups images with the same semantic category, such as isolated objects, objects within scenes, and standalone scenes.

E. More results

We provide more pictures for comparison of our approach D3DR against other methods. Each scene has 32 pictures, where 16 represent the full rendered image, and other 16 represent zoomed images to better observe the object.

The prompts used for generation are:

- For bathroom_1, *object-desc* is *caution wet floor sign*, *scene-desc* is *bathroom*, y_{tgt} is *a caution wet floor sign in a bathroom*
- For bathroom_2, *object-desc* is *laundry basket*, *scene-desc* is *bathroom*, y_{tgt} is *a laundry basket in a bathroom*
- For bedroom_1, *object-desc* is *pillow*, *scene-desc* is *bedroom*, y_{tgt} is *a pillow on a bed in a bedroom*
- For bedroom_2, *object-desc* is *vase*, *scene-desc* is *bedroom*, y_{tgt} is *a vase in a bedroom*
- For kitchen_1, *object-desc* is *suitcase*, *scene-desc* is *room*, y_{tgt} is *a suitcase on a sofa in a room*
- For kitchen_2, *object-desc* is *cup*, *scene-desc* is *kitchen*, y_{tgt} is *a cup on a table in a kitchen*
- For living_room_1, *object-desc* is *parrot statue*, *scene-desc* is *living room*, y_{tgt} is *a parrot statue in a living room*
- For living_room_2, *object-desc* is *piano*, *scene-desc* is *living room*, y_{tgt} is *a piano in a living room*
- For office_1, *object-desc* is *office chair*, *scene-desc* is *office*, y_{tgt} is *a office chair in an office*
- For office_2, *object-desc* is *dumbbell*, *scene-desc* is *office*, y_{tgt} is *a dumbbell on a table in an office*



Figure 8. **Tiny dataset of 4 images** This dataset represent the object (cup) in the scene (room) under various illumination conditions.



Figure 9. **Raw object insertion.** We use tiny dataset to perform raw insertion of the cup in the scene with inconsistent lighting condition.

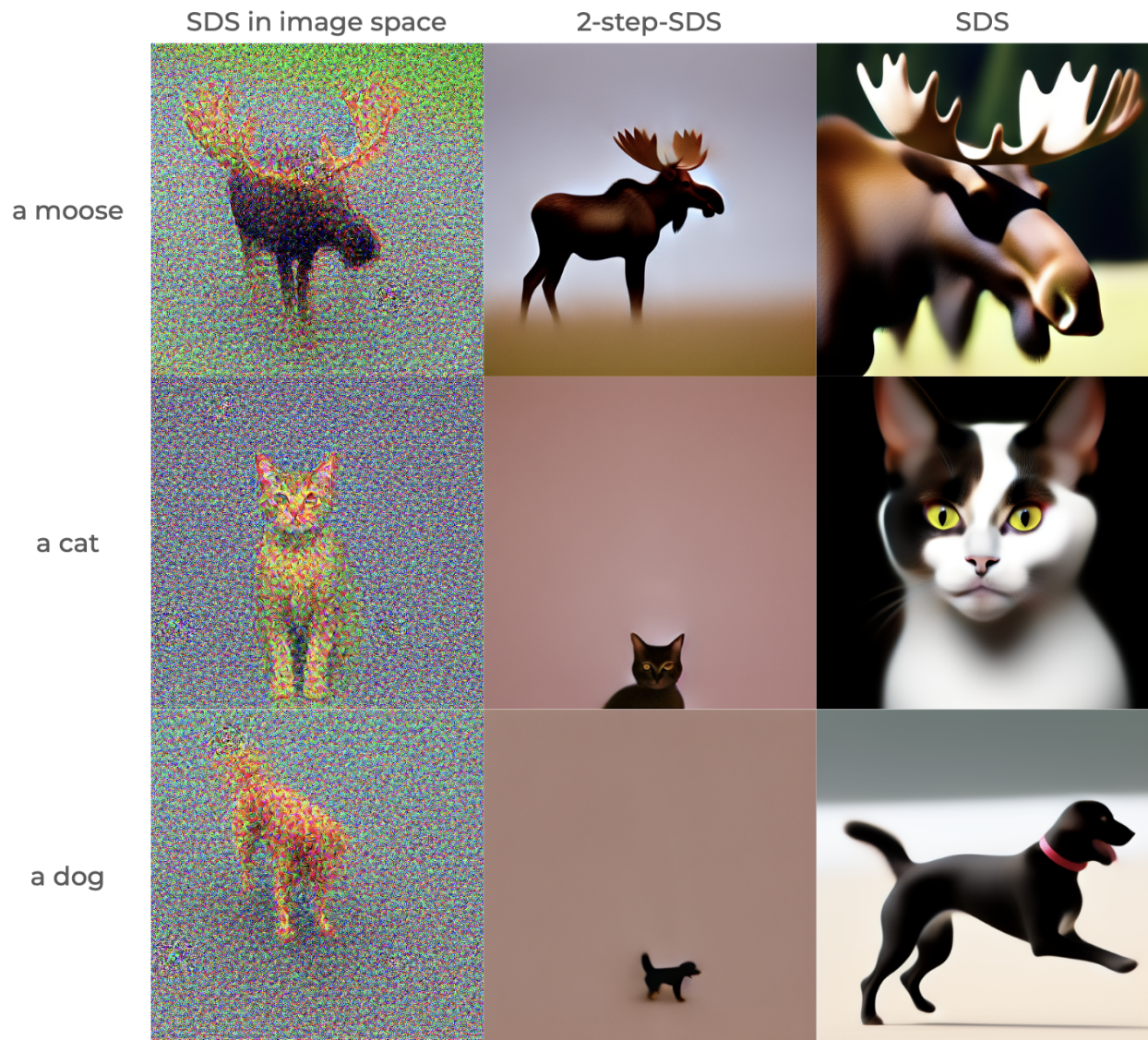


Figure 10. **2-step-SDS generation.** The first column shows results from classical SDS optimization in image space, the second column presents our 2-step-SDS optimization, and the third column illustrates classical SDS optimization in latent space. Each row corresponds to a different prompt.

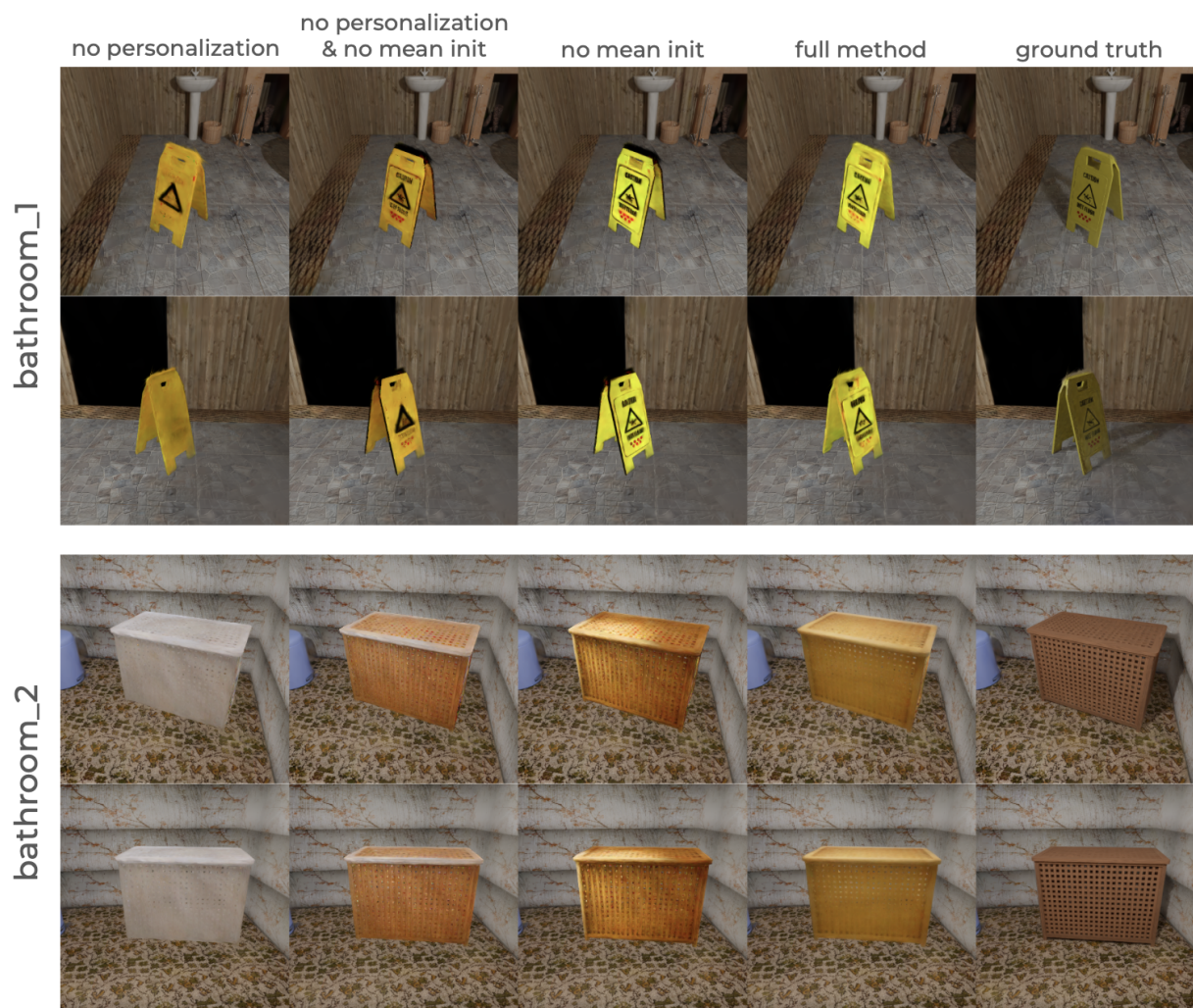


Figure 11. **Ablation studies.** The figure illustrates the impact of personalization and mean initialization on object appearance and texture preservation.



Figure 12. **Comparison on bathroom.1.** The left side displays full rendered images using different methods, while the right side presents zoomed-in views for a closer examination of the object. Each column corresponds to the same method, and each row represents the same camera pose. TIP-Editor does not generate the object. R3DG object has a black border.

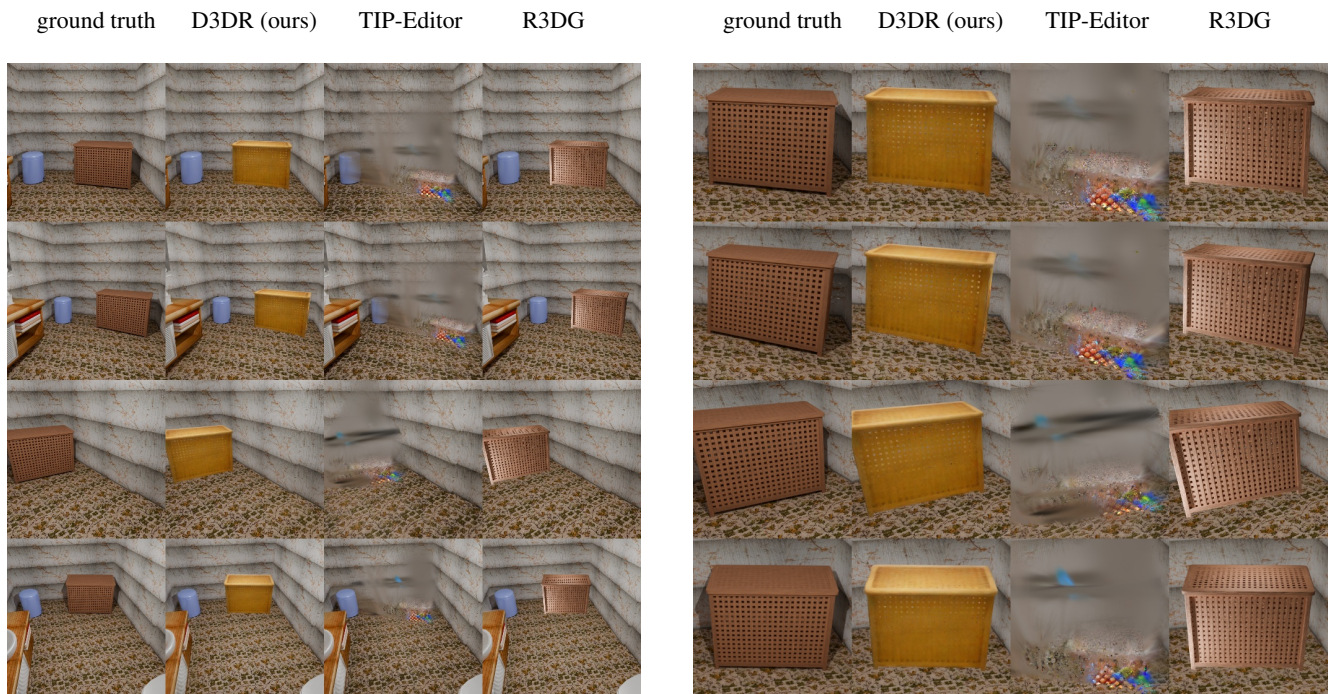


Figure 13. **Comparison on bathroom.2.** TIP-Editor generated the head of the laundry basket.

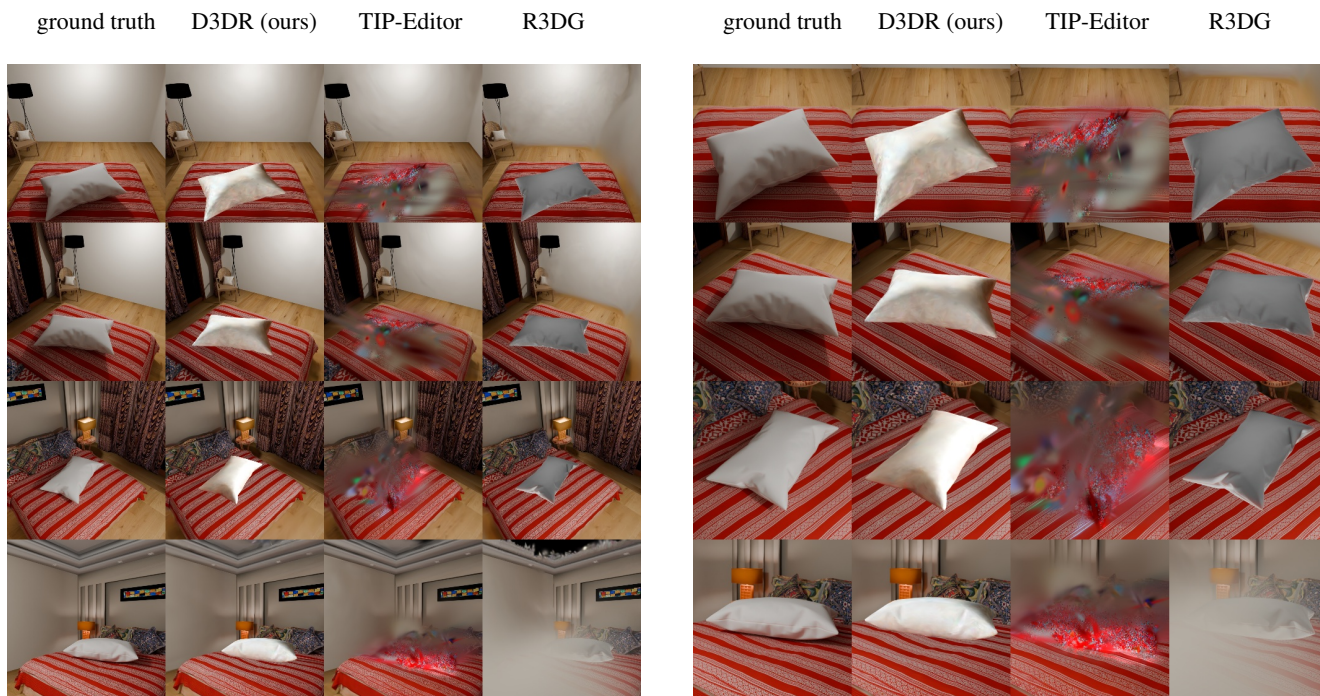


Figure 14. **Comparison on bedroom_1.** TIP-Editor does not converge to a meaningful pillow. R3DG produces a more bright pillow but has realistic shadows in comparison to other methods.

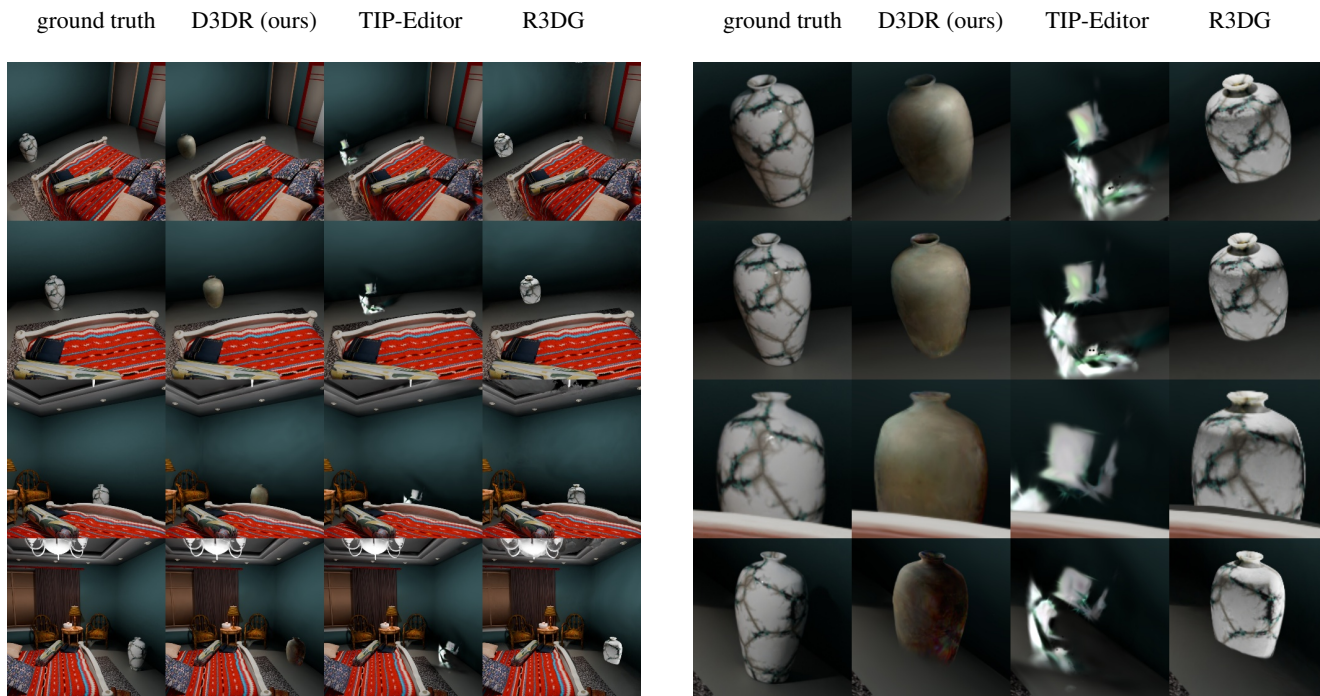


Figure 15. **Comparison on bedroom_2.** TIP-Editor struggles to generate a full vase. R3DG has not produced object relighting, i.e. the object appearance remains the same as it was before insertion. D3DR struggles in reconstruction of the difficult vase texture

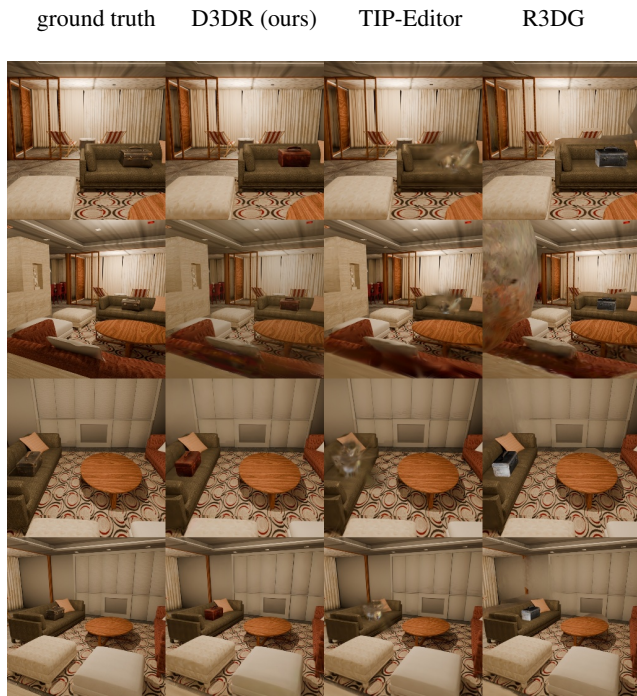


Figure 16. **Comparison on kitchen_1.** TIP-Editor does not converge. R3DG adjusts the object appearance on a negligible value. D3DR produces suitcase with a different color and finds realistic shadows.

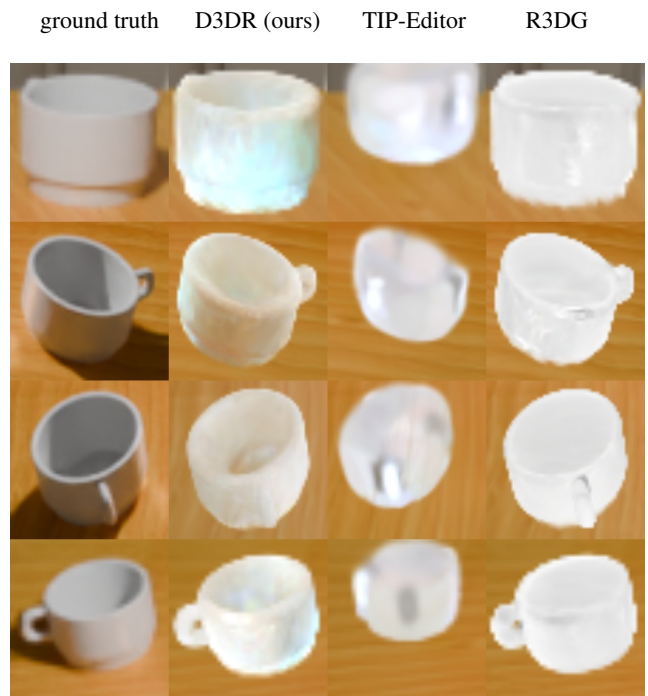
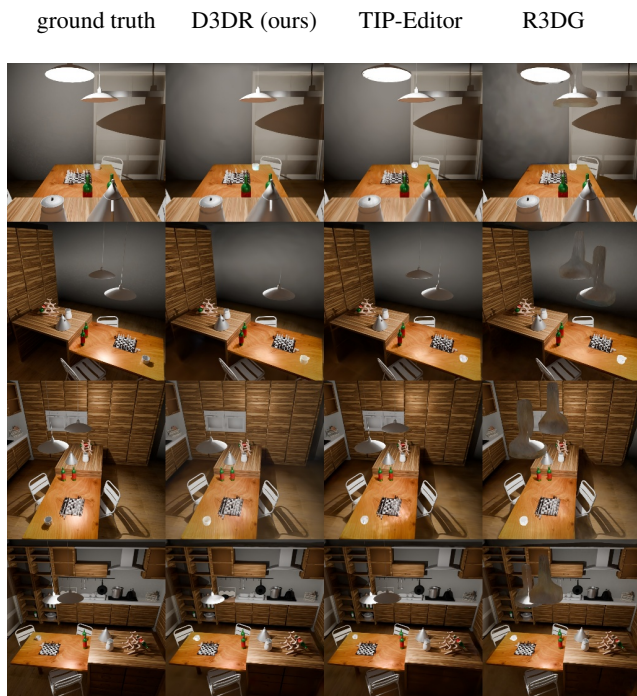


Figure 17. **Comparison on kitchen_2.** TIP-Editor successfully generates a small object (cup), but it does not preserve the object's geometry

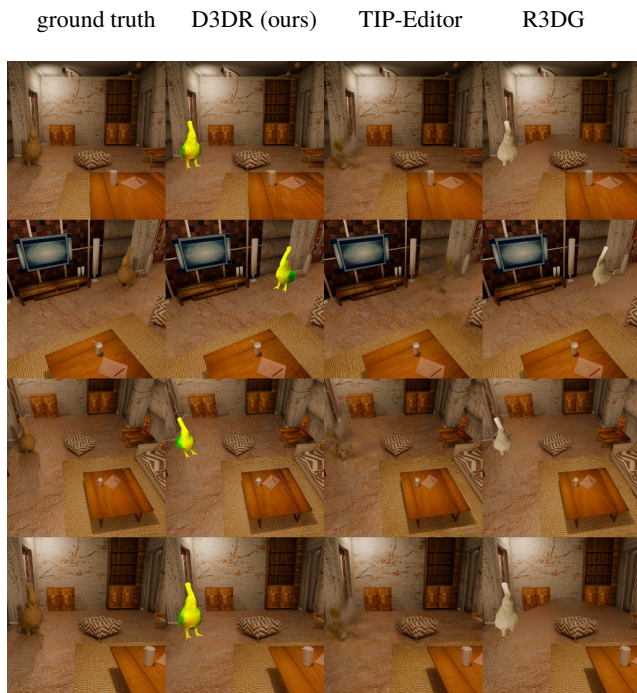


Figure 18. Comparison on living_room.1. D3DR generates wrong textures because the personalization step fails.

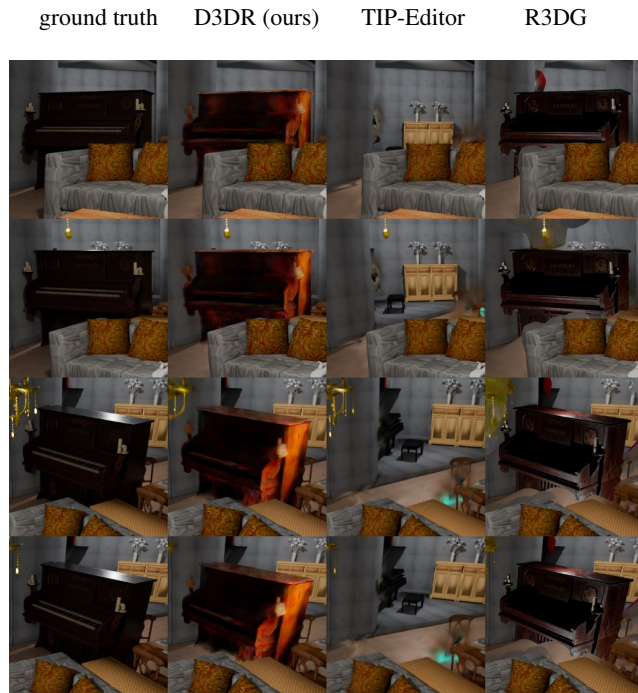
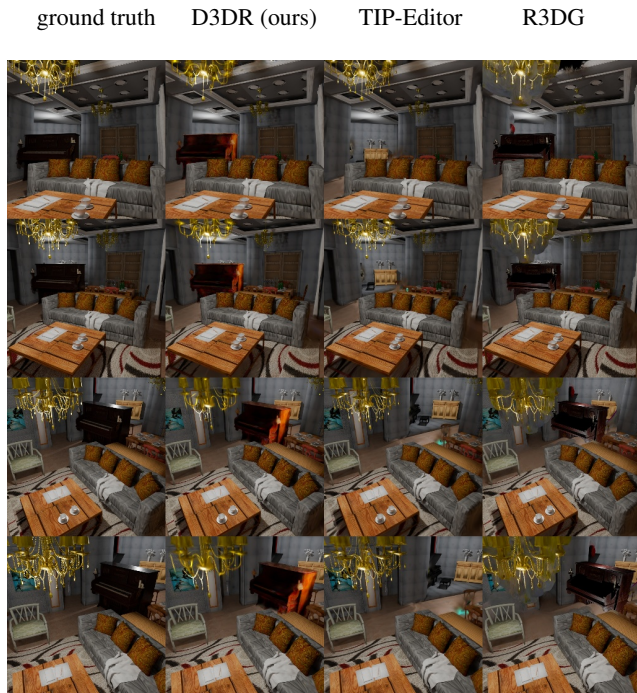


Figure 19. Comparison on living_room.2. TIP-Editor failed to generate such a big 3D object

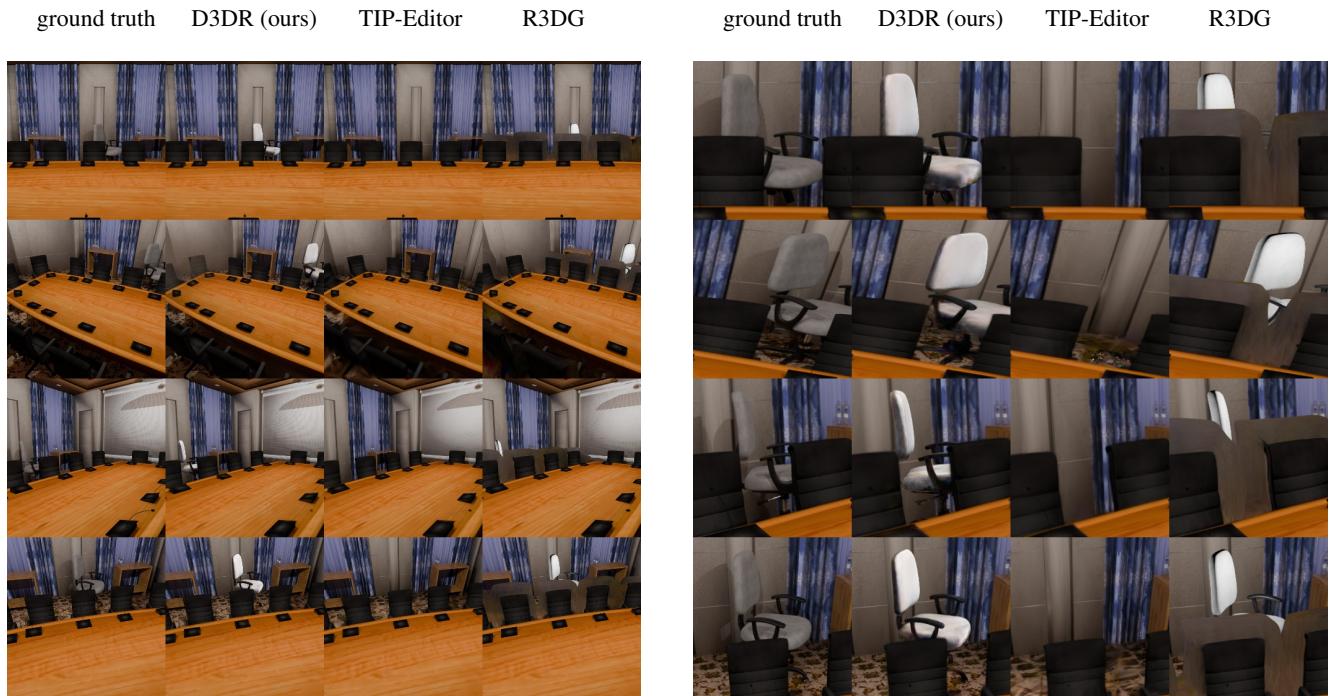


Figure 20. **Comparison on office_1.** TIP-Editor does not generate the office chair. D3DR generates a slightly brighter chair which has realistic appearance

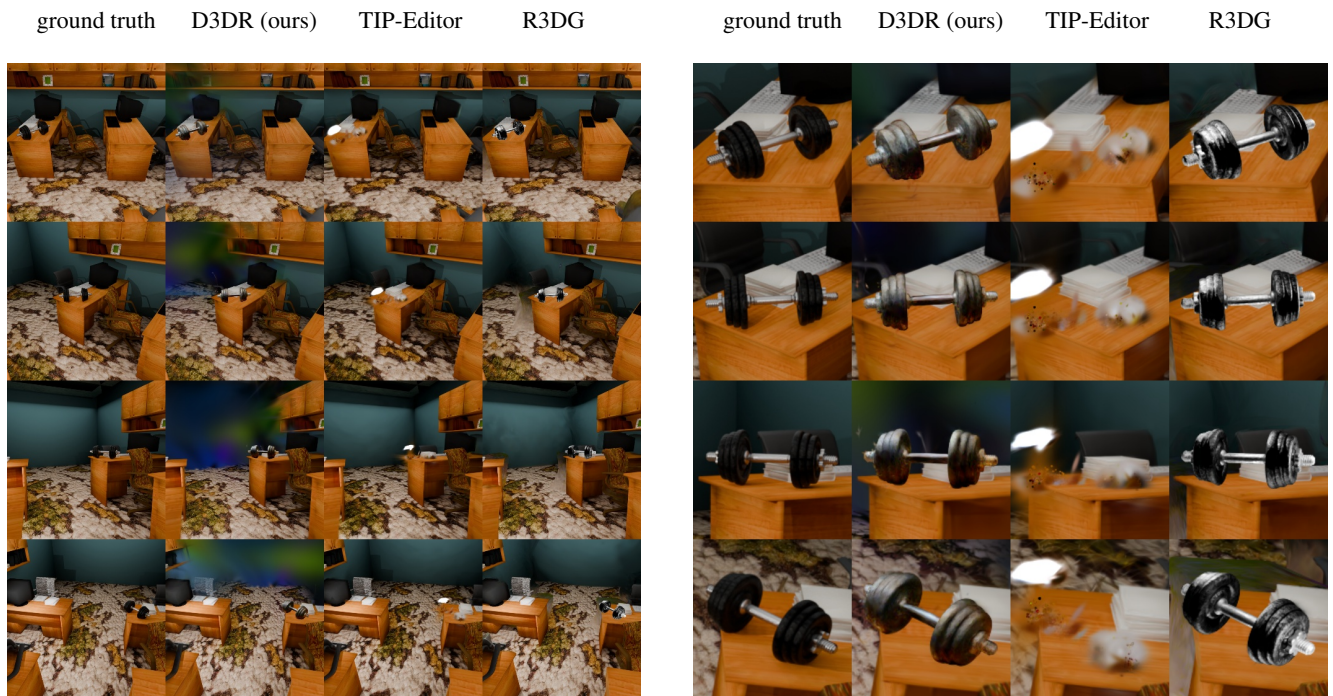


Figure 21. **Comparison on office_2.** TIP-Editor generates only a part of the dumbbell.